ACS Biomaterials SCIENCE & ENGINEERING

pubs.acs.org/journal/abseba

Article

# Surface-Enhanced Raman Scattering-Active Gold-Decorated Silicon Nanowire Substrates for Label-Free Detection of Bilirubin

Anna D. Kartashova, Kirill A. Gonchar, Dmitry A. Chermoshentsev, Ekaterina A. Alekseeva, Maxim B. Gongalsky, Ivan V. Bozhev, Andrei A. Eliseev, Sergey A. Dyakov, Jeanne V. Samsonova, and Liubov A. Osminkina*

Cite This: *ACS Biomater. Sci. Eng.* 2022, 8, 4175–4184

Read Online

ACCESS | Metrics & More | Article Recommendations | Supporting Information



**ABSTRACT:** Bilirubin (BR) is a product of hemoglobin breakdown, and its increasing levels in the blood may indicate liver disorders and lead to jaundice. Kernicterus is most dangerous in newborns when the unconjugated BR concentration can quickly rise to toxic levels, causing neurological damage and even death. The development of an accurate, fast, and sensitive sensor for BR detection will help reduce diagnostic time and ensure successful treatment. In this study, we propose a new method for creating a surface-enhanced Raman scattering (SERS)-active substrate based on gold-decorated silicon nanowires (Au@SiNWs) for sensitive label-free BR detection. Gold-assisted chemical etching of crystalline silicon wafers was used to synthesize SiNWs, the tops of which were then additionally decorated with gold nanoparticles. The low detection limit of model analyte 4-mercaptopyridine down to the concentration of $10^{-8}$ M demonstrated the excellent sensitivity of the obtained substrates for SERS application. The theoretical full-wave electromagnetic simulations of Raman scattering in the Au@SiNW substrates showed that the major contribution to the total SERS signal comes from the analyte molecules located on the SiNW surface near the gold nanoparticles. Therefore, for efficient BR adsorption and SERS detection, the surface of the SiNWs was modified with amino groups. Label-free detection of BR using amino modified Au@SiNWs with high point-to-point, scan-to-scan, and batch-to-batch reproducibility with a detection limit of $10^{-6}$ M has been demonstrated. Artificial urine, mimicking human urine samples, was used as the matrix to get insights into the influence of different parameters such as matrix complexity on the overall BR SERS signal. The signal stability was demonstrated for 7 days after adsorption of BR with a concentration of $5 \times 10^{-5}$ M, which is the required sensitivity for clinical applications.

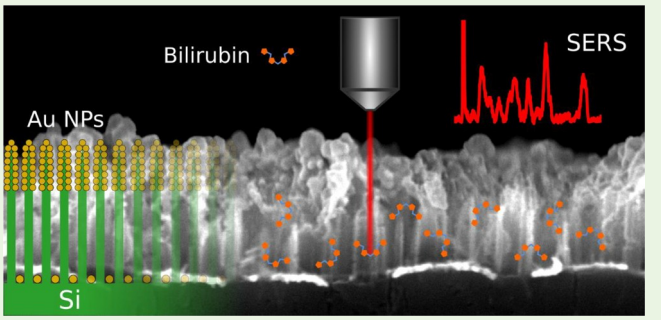


**KEYWORDS:** *bilirubin, gold-decorated silicon nanowires, label-free SERS detection, jaundice, sensor*

## INTRODUCTION

Bilirubin (BR) is a breakdown product of heme catabolism in aged red blood cells in all mammals. Free BR is toxic yellow tetrapyrrol, which exists in human serum as an unconjugated form and has a lipophilic nature.[1] In the blood circulatory system, most of the unconjugated BR is tightly bound to serum albumin; then, it is conjugated in the liver with glucuronic acid and is excreted in the bile.[2] The human neonate has an undeveloped capability of conjugation and excretion and, consequently, accumulates BR in the blood plasma. This results in yellow staining of the skin, icterus neonatorum, and usually subsides in the course of several days.[2,3] Kernicterus is most dangerous in newborns when the free BR concentration quickly rises to toxic levels, causing neurological damage and even death.[4,5] An increase in the level of free BR in the blood can also be diagnosed in an adult due to liver problems caused by infections (hepatitis A), pathologies (Gilbert's syndrome, Rotor syndrome, etc.), or diseases (e.g., cirrhosis of the liver).[6]

The normal level of free BR is <25 $\mu$M (<12 mg/L) in healthy human blood,[7,8] and it plays the role of a potent physiological antioxidant that may provide important protection against atherosclerosis, coronary artery disease, and inflammation. A low concentration of BR is associated with coronary artery disease and iron deficiency.[9] At high levels of free BR (>50 $\mu$M, >25 mg/L), the so-called hyperbilirubinemia leads to jaundice, hepatitis, mental disorders, cerebral palsy, brain damage, and death (especially in the case of neonates).[5,10,11] Therefore, the development of an accurate,

**Special Issue:** Advances on Porous Nanomaterials for Biomedical Application (Drug Delivery, Sensing, and Tissue Engineering)

**Received:** May 31, 2021
**Accepted:** October 27, 2021
**Published:** November 14, 2021

rapid, and sensitive sensor for BR detection is an urgent task that will help reduce diagnostic time and ensure successful treatment.

The problem of finding an accurate and specific method to determine the BR level has long attracted the attention of specialists. Historically, Ehrlich in 1883 treated BR in urine with diazo reagent and described the formation of a red-blue colored pigment. Later, Van den Bergh and Muller found that BR in normal serum reacts with Ehrlich's diazo reagent (diazotized sulfanilic acid).[11] Currently, the most common methods for the determination of BR in blood serum in the clinic are direct spectroscopic measurement and the method of the diazo reaction.[11−13] However, direct spectroscopic measurements can be inaccurate due to interference with other heme proteins, including carotenoids, which absorb light at the same wavelengths. The pH dependence of the diazo reaction reduces the accuracy of this method.[14]

Surface-enhanced Raman scattering (SERS) has been proven to successfully detect different biomarkers of diseases, viruses, bacteria, etc.[15−17] SERS was first observed by Martin Fleischmann and his co-workers during their measurements of Raman scattering, inelastic light scattering, on the surface of a rough silver electrode in 1974.[18] Due to the SERS effect, the intensity of Raman scattering of light by molecules adsorbed on the nanostructured surfaces of noble metals usually increases by 6−8 orders of magnitude. The observed increase in Raman intensity can be explained by two mechanisms: electromagnetic, which is associated with localized surface plasmon resonance in the nanostructures of noble metals, and chemical, caused by the charge transfer between adsorbed molecules and the nanostructures.[15,19] The main characteristics of a proper SERS substrate are its homogeneity and batch-to-batch reproducibility; the stability of the SERS signal intensity and easy and cost-effective fabrication are also needed.

There are several reports describing the detection of BR using SERS-active substrates; for example, a graphene isolated Au nanocrystal, loaded on cellulose paper strips, has demonstrated the ability to detect BR directly from a newborn baby patient with jaundice.[20] Geng et al. developed a recyclable SERS substrate by modifying functional boron nitride monolayer nanosheets on silver nanoarrays for label-free detection of BR in complex biological samples.[21] A graphene oxide−gold nanostar hybrid was loaded on filter paper for label-free SERS detection of serum BR.[22] The Ag@$Fe_2O_3$ hybrid substrate was successfully applied to detect bilirubin in human blood.[23] However, despite the observed low detection limit of BR, the signal homogeneity is not well demonstrated, and the process of manufacturing the SERS substrates seems to be challenging. Also, the direct contact between the metal and BR will produce unnecessary light/chemical reactions, which will cause deformation of the molecular structure.[21] Thus, the task of developing easily synthesized highly sensitive substrates with good signal reproducibility for label-free SERS diagnostics of BR does not lose its relevance.

Arrays of silicon nanowires (SiNWs) are attractive objects for creating sensitive sensors due to the simplicity of their preparation methods and silicon surface tailorability.[24−26] Since arrays of nanowires have a huge surface area, a high number of metallic nanoparticles (NPs) could be packed on them, which would yield a high enhancement factor when using such nanostructures as SERS-active substrates.[27,28] For example, a hybrid photonic/plasmonic platform based on gold-decorated porous silicon with surface biofunctionalization by polyelectrolytes, which are engineered with bioreceptors to enable label-free detection of target analytes, was proposed by Mariani et al.[29,30]

SiNWs can be obtained by several different methods, but among them, metal-assisted chemical etching is the simplest method that does not require expensive equipment and is attracting more and more attention in the large-scale production of SiNWs.[28,31] Usually, silver-assisted chemical etching is used to obtain SiNW arrays, and in most cases, the surface of the nanowires is also decorated with silver nanoparticles (Ag NPs) to provide them the properties of SERS activity.[28] However, the stability of the enhancement factor for the Raman signal of such substrates is not obvious due to the tendency of Ag NPs to oxidize with the release of ions and ROS,[32] which can rapidly occur when nanoparticles interact with biological fluids and can also adversely affect the studied bioanalytes.

In the current study, we present SERS-active gold-decorated SiNW (Au@SiNW) substrates for label-free detection of BR for the first time. We propose a new method for producing SiNWs in which gold nanoparticles (Au NPs), directly reduced on a crystalline silicon wafer from a solution of gold chloride and hydrofluoric acid, are used as catalysts for a chemical reaction in metal-assisted chemical etching (MACE). To achieve SERS activity of the obtained substrates, the tops of the nanowires are additionally coated with Au NPs. The low detection limit of the model analyte 4-mercaptopyridine down to $10^{-8}$ M demonstrated the superior sensitivity of Au@SiNW for SERS applications. It is shown that the modification of the surface of the SiNWs with amino groups provides hydrophobization of the SERS substrates and effective adsorption of bilirubin. Label-free detection of BR using amino modified Au@SiNWs up to concentrations of $10^{-6}$ M has been demonstrated. Artificial urine matrix (AUM) simulating human urine samples and human serum albumin (HSA) solution were used to gain insight into the effect of various parameters, such as matrix complexity, on the overall SERS BR signal. Signal stability is shown for 7 days after adsorption of BR from the AUM with a concentration of $5 \times 10^{-5}$ M, which is the required sensitivity for clinical applications. This, together with the ease of the developed method for the production of Au@SiNWs, high point-to-point, scan-to-scan, and batch-to-batch reproducibility of the BR signal, and the sensitivity required for clinical applications, opens the possibility of using this SERS-active substrates as platforms for point-of-care clinical diagnostics.

## MATERIAL AND METHODS

**Chemicals.** Hydrofluoric acid 48% (HF), hydrogen peroxide ($H_2O_2$, 30%), isopropanol, and acetone were purchased from Mosreactiv, Russia. 50% gold(III) chloride ($AuCl_3(H_2O)_2$) from ABCR, Germany, and 3-aminopropyl(triethoxyl)silane (APTES) from Gelest, USA, were used. $CaCl_2$, $Na_2SO_4$, $MgSO_4$, $NH_4Cl$, KCl, urea, $NaH_2PO_4{\cdot}2H_2O$, $Na_2HPO_4$, sodium citrate, NaCl, 4-mercaptopyridine (4MPy, 95%), human serum albumin (HAS) powder (>98%), bilirubin (BR) powder (>98%), and phosphate-buffered saline (PBS) were purchased from Sigma-Aldrich, Germany.

**Fabrication of Gold-Decorated Silicon Nanowires.** The SiNW arrays were created by metal-assisted chemical etching (MACE) of 1−5 Ωcm boron-doped single crystalline silicon (c-Si) wafers (Silicon Materials, Germany). First, before the MACE procedure, the c-Si wafers were rinsed in acetone and isopropanol


https://doi.org/10.1021/acsbiomaterials.1c00728
ACS Biomater. Sci. Eng. 2022, 8, 4175−4184

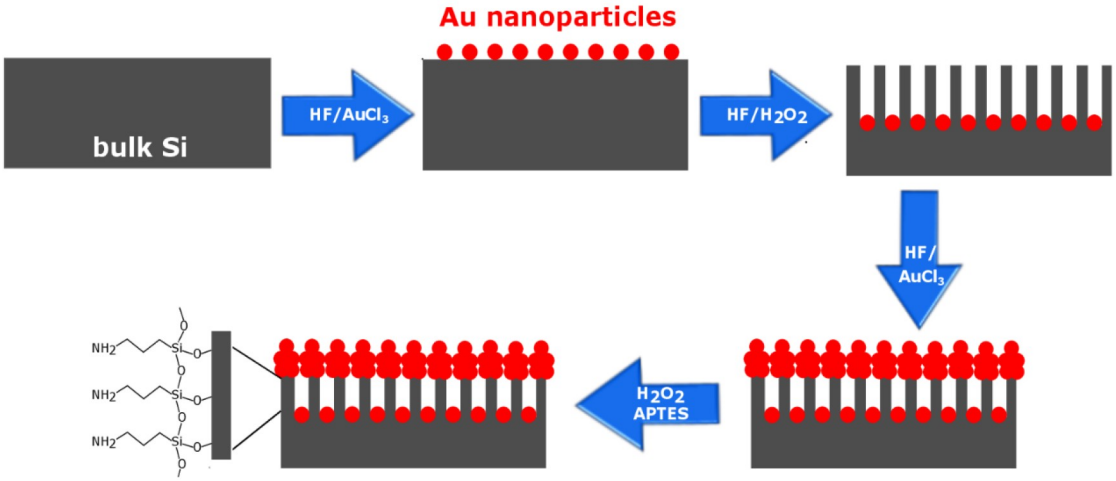


**Figure 1.** Schematic representation of the formation of Au@SiNWs substrates and their subsequent surface modification.

in an ultrasound bath (Elmasonic S, Germany) for 2 min to remove organic and inorganic residues and then rinsed in 5 M HF aqueous solution to remove the native oxide. In the first step of MACE, gold nanoparticles (Au NPs) were deposited on the c-Si surfaces by immersing them in an aqueous solution of 0.01 M $AuCl_3$ and 5 M HF at a volume ratio of 1:1 for 30 s. In the second step, the c-Si surfaces covered with Au NPs were immersed in the second etching solution containing 5 M HF and 30% $H_2O_2$ at a volume ratio of 10:1 in a Teflon vessel for 3 min. The etching step was performed at room temperature (RT). After the MACE procedure, the typical SiNW arrays of vertically aligned nanowires with native Au NPs at the bottom were obtained, as schematically shown in Figure 1.

To deposit Au NPs at the top of SiNWs, the substrates were immersed in 0.01 M $AuCl_3$ and 5 M HF at a volume ratio of 1:1 for 30 s at RT (Figure 1). Finally, the samples were rinsed several times in deionized water and dried at room temperature. After fabrication, a silicon wafer with the Au@SiNWs layer was cut into 5 × 5 mm chips. Note that more than 200 chips are obtained from one 4 in. silicon wafer.

**Sample Characterization.** The scanning electron microscope (SEM; Zeiss Supra-40, Germany) was used to study the morphology and composition of the obtained Au@SiNWs substrates. Energy dispersive X-ray fluorescence spectroscopy was performed using a M1 Mistral Micro-X-ray fluorescence analyzer equipped with an Rh target and 30 $mm^2$ Peltier cooled silicon drift detector (Bruker, Germany). For area-averaged spectra, the collimator was set to 1.5 mm excitation. The specular reflection spectra of the Au@SiNW substrates before and after the modification process with the amino groups were measured in the range of 800−1900 $cm^{-1}$ using a Bruker IFS 66v/S FT-IR spectrometer, Germany, at an incidence angle of 13° at a pressure of 2 mbar.

**SERS Measurements of 4-Mercaptopyridine.** To verify the ability of the obtained substrates to amplify the Raman signal, 4-mercaptopyridine (4-MPy) was used. First, stock solutions of $10^{-4}$ M for 4-MPy were prepared in high-purity water by adding the appropriate amount of powder. Next, stock solutions were diluted to final concentrations of $10^{-5}$−$10^{-8}$ M. For the SERS measurements, the samples were incubated for 30 min in the as-prepared solutions of the analytes and then air-dried. The SERS measurements were performed using a commercially available Confotec MR350 Raman spectrometer (SOL Instruments, Belarus) equipped with a 633 nm laser. During the measurements, a 600 lines/mm grating was used, and a 50× Zeiss objective (N.A. 0.65; W.D. 1.6 mm) was employed to focus the laser beam on the sample and to collect the backscattered light. Focusing was carried out according to the signal intensity. The laser power at the surface of the sample was 0.5 mW. For every substrate, 3 different areas of 10 × 10 $\mu$m size were measured using a 1 $\mu$m step; this resulted in 300 spectra per scan. Scan areas were chosen randomly at a significant distance from each other. The integration time for every spectrum was 30 s.

**Silicon Nanowire Surface Modification.** For efficient adsorption of bilirubin (BR), the surface of the SiNWs was modified with amino groups (−$NH_2$). The procedure was similar to that described in a previous work.[33] The Au@SiNW substrates were thoroughly washed in ethanol and then in ultrapure water for 5 min using an IKA VXR basic Vibrax orbital shaker (Germany) to remove possible contamination from the surface. To attach OH groups, the substrates were immersed in 30% $H_2O_2$ for 30 min; after that, the residues of hydrogen peroxide were washed away by rinsing the substrate for 5 min in ethanol and ultrapure water using the orbital shaker. After air drying, the substrates were immersed in a solution of ethanol and 3-aminopropyl(triethoxyl)silane (APTES) at a ratio of 10:1 overnight (about 17 h) with stirring on an orbital shaker. Finally, the substrates were washed three times on an orbital shaker in ethanol for 10 min. The modified substrates were dried in a closed Petri dish. A schematic representation of the surface modification of the SiNWs is shown in Figure 1.

**Measurement of the Substrates' Surface Hydrophobicity.** Hydrophilicity and hydrophobicity of the Au@SiNW substrates before and after the modification process was studied by contact angle measurements using a self-made system equipped with an optical microscope MicMed 5.0 300× (Russia). For this, a drop (5 $\mu$L) of phosphate-buffered saline (PBS) was placed onto the surface of the samples and the angle between the solid−liquid interface was measured once equilibrium was reached.

**SERS Measurements of Bilirubin.** Since BR is hydrophobic, its powder was first diluted with dimethyl sulfoxide (DMSO) to a concentration of $10^{-2}$ M. All actions with the BR were carried out in a dark room with a red-light source since BR tends to photodegrade under sunlight. The DMSO solution then was diluted in PBS down to BR concentrations of $10^{-4}$−$10^{-6}$ M. The Au@SiNW substrates were incubated in solutions for 2 h in a dark place and dried in air, and the Raman measurements were immediately taken. The same measurement conditions were used as described above for 4-MPy. For every substrate, 3 different areas of 10 × 10 $\mu$m size were measured using a 1 $\mu$m step; this resulted in 300 spectra per scan. Scan areas were chosen randomly at a significant distance from each other. The integration time for every spectrum was 15 s, and the laser power was 1 mW.

To measure the selectivity of the developed platform, the presence of BR was evaluated in a model solution with competing human serum albumin (HSA) molecules. HSA was added into PBS or into a PBS solution of BR with concentrations of $10^{-5}$ M to achieve an albumin concentration of $10^{-4}$ M. The Au@SiNW substrates were incubated with a solution of HSA or with an HSA and BR solution,


https://doi.org/10.1021/acsbiomaterials.1c00728
ACS Biomater. Sci. Eng. 2022, 8, 4175−4184

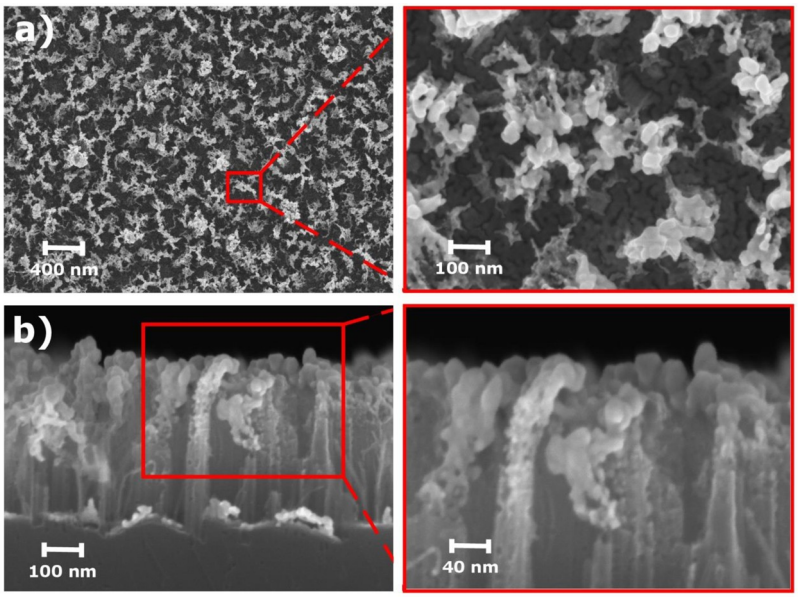


**Figure 2.** SEM images of the Au@SiNW substrates: (a) top-view; (b) cross-sectional view.

and the SERS signals were measured in the same way as described above.

An artificial urine matrix, simulating human urine, was used to gain insight into the effect of various parameters, such as matrix complexity, on the overall SERS BR signal. Artificial urine was synthesized according to a modified protocol published by Hidi et al.[34] Briefly, the aqueous solution contains 13.72 mM $CaCl_2$, 34.21 mM $Na_2SO_4$, 5.92 mM $MgSO_4{\cdot}7H_2O$, 85.99 mM $NH_4Cl$, 162.71 mM KCl, 832.5 mM urea, 17.05 mM $NaH_2PO_4{\cdot}2H_2O$, 7.25 mM $Na_2HPO_4$, 5.46 mM sodium citrate, and 23.69 mM NaCl and has a pH value of 5. The DMSO solution of BR with a concentration of $10^{-2}$ M was then diluted in the AUM down to BR concentrations of $5 \times 10^{-5}$ M. The Au@SiNW substrates were incubated in solutions for 2 h in a dark place and dried in air in the dark, and the Raman measurements were taken immediately and after 1, 2, 3, 5, and 7 days of storing the sample in the dark at 4 °C.

**Simulation of Surface-Enhanced Raman Scattering.** The simulations of SERS near SiNW and Au@SiNW substrates were carried out using the finite element method (FEM) in COMSOL Multiphysics.

**Processing of Results.** Raman spectra were processed using Origin and Excel. Raman intensities from three maps (300 scans) for each substance and each concentration were averaged, and the mean deviation was calculated. The water contact angles from the obtained images of the PBS drops were determined using the Contact Angle plugin in ImageJ.

## RESULTS AND DISCUSSION

**Characterization of the Au@SiNW Substrates.** Figure 2 shows planar and cross-sectional SEM images of the obtained Au@SiNW substrates. According to the presented micrographs, as a result of the Au-assisted chemical etching, arrays of nanowires with a diameter of about 50 nm are formed. The nanowire layer thickness for the chosen etching time of 3 min was 400 nm. 50−100 nm agglomerates of gold nanoparticles (Au NP) about 20 nm in diameter, which act as catalysts for the chemical etching reaction of the crystalline silicon substrate, are seen in Figure 2b at the base of the SiNWs. Thus, the distance between the nanowires was also 50−100 nm.

The gold coating of the SiNWs was performed at room temperature by chemical deposition of the Au NPs due to the reduction of gold(III) chloride ($AuCl_3$) in HF.[35] It can be seen from SEM cross-sectional microphotographs that Au NPs cover the tops of the nanowires and form branched structures consisting of nanoparticles of about 20 nm in size. During the deposition of Au NPs, the tops of the nanowires are partially etched, and the nanoparticles literally adhere to the nanowire. The thickness of the top layer of the nanowires decorated with gold is about 120 nm.

The presence of gold in both the initial silicon nanowire substrates after Au-assisted chemical etching and the Au@SiNW substrates after additional gold layer deposition was confirmed with energy dispersive X-ray fluorescence spectroscopy (Figure S1). Both the samples indicate well-defined emission from Au L-line series with an intensity growing ∼1.5 times in the sample with the top gold additional layer. When one assumes an attenuation length of Au of ∼5 $\mu$m at 10 keV and the thickness of deposited Au NPs of ∼20 nm, the intensity rise can be addressed assuredly to the proportional increase of the gold quantity in the samples.

**Investigation of the SERS Activity of the Au@SiNW Substrates.** To evaluate the SERS activity of the obtained Au@SiNWs, a probe molecule, 4-mercaptopyridine (4-MPy), was used. 4-MPy is a typical aromatic thiol compound consisting of a thiol group (R−S−H) located in the para position with respect to the nitrogen atom in a pyridine ring. This special structure allows it to form well-ordered self-assembled monolayers on metal surfaces, which have great promising uses in many fields such as sensors, catalysts, and optics.[33]

Figure 3 shows the Raman spectrum of the 4-MPy powder and the Au@SiNW substrate as well as the SERS spectra of various concentrations of 4-MPy.

In the SERS spectra of 4-MPy, shown in Figure 3, the peak at 1010 $cm^{-1}$ attributed to the ring breathing mode was enhanced and shifted to the higher wavenumbers compared to the spectrum of the powder. The peak at 1092 $cm^{-1}$ corresponds to the C−H out-of-plane bend, and the one at 1209 $cm^{-1}$ is assigned to the C−H with N−H bending. The peak at 1576 $cm^{-1}$ is attributed to C−C stretching. Insignificant shifts in the SERS spectra in comparison with


https://doi.org/10.1021/acsbiomaterials.1c00728
ACS Biomater. Sci. Eng. 2022, 8, 4175−4184

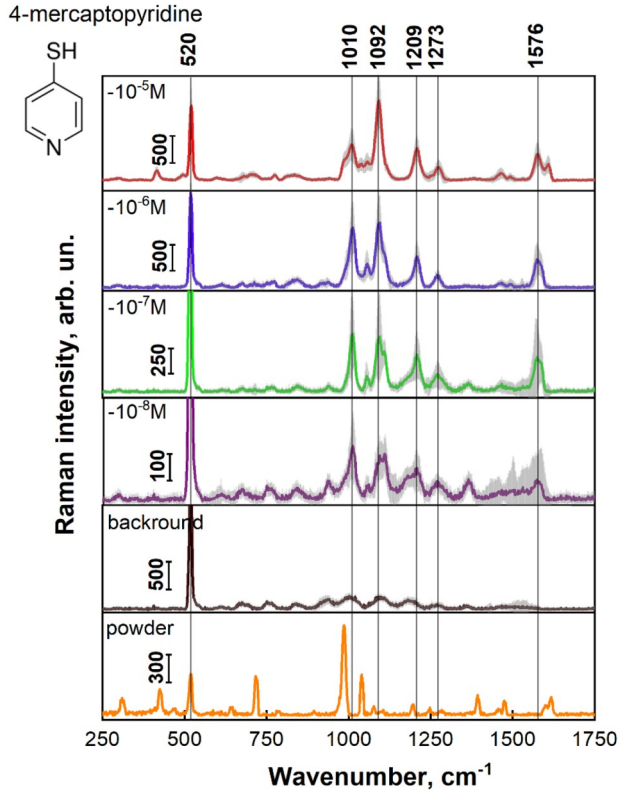


**Figure 3.** Raman spectrum of 4-MPy powder, Au@SiNW substrate (denoted as background), and average SERS spectra of various concentrations of 4-MPy. The gray shading in the average spectra shows the standard deviations calculated from about 300 spectra: 100 spectra each for three different regions of the substrate.

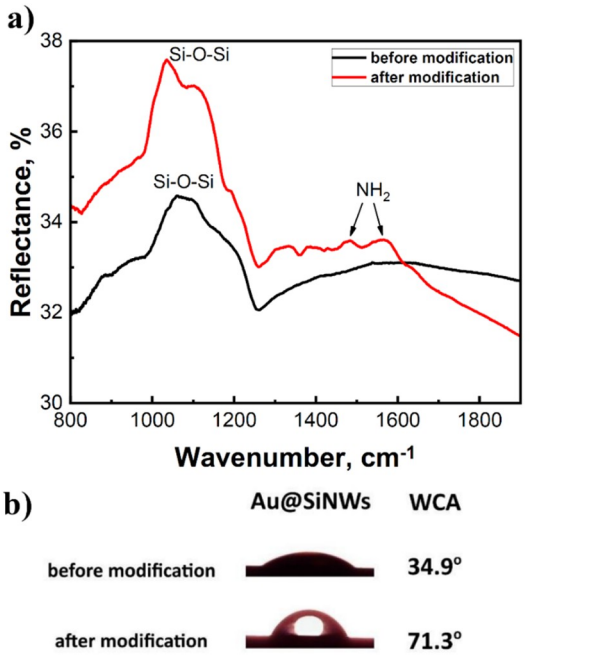


**Figure 4.** Properties of the Au@SiNW surface: (a) IR specular reflectance spectra of the Au@SiNWs before (black) and after (red) modification with amino groups; (b) WCA of PBS drop deposited on the surface of Au@SiNW substrates before and after modification.

the Raman spectrum of 4-MPy powder can be explained by the loss of intramolecular hydrogen bonding, the interaction between 4-MPy and water in solution, and the specific interaction of the molecule with Au NPs.[36,37] According to the data presented, 4-MPy was successfully detected down to the concentration of $10^{-8}$ M. At the same time, the absence of parasitic Raman peaks of the Au@SiNW substrate indicates its purity, and the presence of a crystalline silicon peak at about 520 $cm^{-1}$ allows wavenumber normalization of the SERS spectra. All of this points to the great potential of Au@SiNW substrates for SERS applications.

Note that the 4-MPy detection limit for the SiNW substrate without subsequent gold coating was $10^{-5}$ M (Figure S2). Thus, the additional decoration of SiNW tops with Au NPs provides an increase in the 4-MPy signal by 3 orders of magnitude.

**Surface Modification.** BR is a hydrophobic, negatively charged molecule.[38,39] Thus, for effective adsorption of bilirubin, it is necessary to provide hydrophobization and a positive charge of the Au@SiNWs. Since silicon nanostructures are easily modified, they were silanized with 3-aminopropyl-(triethoxyl)silane (APTES) in order to form the amine-terminated SiNW surface (Figure 1). This provided a positive charge of the nanowire surface.[39]

Infrared (IR) specular reflectance spectra of the Au@SiNWs before and after the modification process are presented in Figure 4a. Si−O−Si stretching modes in the range of 1050−1150 $cm^{-1}$ indicate the presence of silicon oxide on the surface of the nanowires before and after the modification process. The appearance of modes at 1484 and 1564 $cm^{-1}$, which are associated with the deformation modes of the $NH_2$ amino groups[40,41] in the samples after APTES treatment, indicate the successful modification of the sample surface.

To determine how the modification affects the hydrophilicity/hydrophobicity of Au@SiNW, the water contact angles (WCAs) of the unmodified and modified substrates were measured. A drop of PBS (5 $\mu$L) was placed onto the surface of the samples, and the angle between the solid−liquid interface was measured once equilibrium was reached. Figure 4b shows that the surface of the unmodified substrate is hydrophilic with a WCA of 34.9°, and after chemical modification, it is more hydrophobic, as evidenced by changes in the WCA to 71.3°.

Thus, the properties of Au@SiNW substrates, acquired after the described process of the chemical modification, as well as the electrostatic interaction between the positively charged amino group of the SiNWs and the carboxyl anion of BR[39] will ensure its effective adsorption.

**SERS Detection of Bilirubin.** Figure 5 shows the Raman spectra of the BR powder, PBS, in which bilirubin was diluted as well as the mean SERS spectra of various concentrations of BR adsorbed on modified Au@SiNW substrates. The SERS spectra clearly show characteristic Raman BR bands: the dominant mode at 685 $cm^{-1}$ corresponds to the twisting of the C═O bond in the COOH group, the peak at 755 $cm^{-1}$ is assigned to out-of-plane ring deformation, and the weak peak at 826 $cm^{-1}$ is due to the ring vibrations;[42,43] the band at 941 $cm^{-1}$ is assigned to out-of-plane C−H bending mode presumably coupled to a stretching C−$CH_3$ mode,[44] and the peak at 986 $cm^{-1}$ corresponds to an asymmetric C−$H_3$ deformation.[43] As can be seen, the characteristic triple peak from the BR powder spectrum at 1247−1290 $cm^{-1}$, which corresponds to oscillating C−H vibrations,[44] tends to merge into a double peak at 1249 and 1292 $cm^{-1}$ in the SERS


https://doi.org/10.1021/acsbiomaterials.1c00728
ACS Biomater. Sci. Eng. 2022, 8, 4175−4184

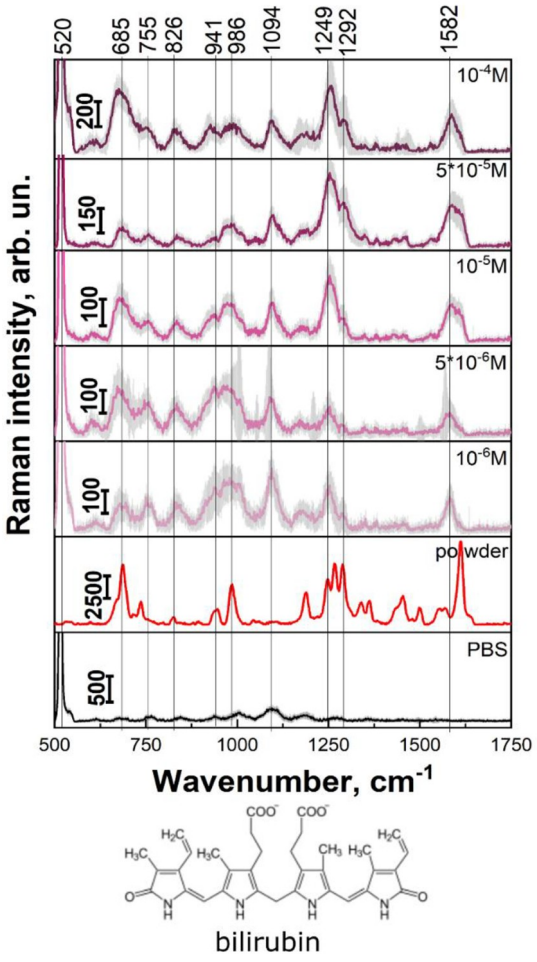


**Figure 5.** Raman spectrum of BR powder and average SERS spectra of various concentrations of BR. The gray shading in the average spectra shows the standard deviations calculated from about 300 spectra: 100 spectra each for three different regions of the substrate.

spectrum. The bands at 1611 and 1570 $cm^{-1}$ in the Raman spectra of the BR powder is assigned to aromatic C−C stretching and asymmetric C−N stretching in a ring[42,43] and merge into one band at 1582 $cm^{-1}$ in the SERS spectra. Note that, according to the data obtained, the signal from PBS was insignificant and did not contribute to the spectra of BR.

The limit of detection (LOD) for BR was determined at the signal-to-noise ratio of 3 and amounted to $10^{-6}$ M. See the details of the estimation in Figures S3 and S4. Note that this sensitivity of the developed Au@SiNW substrates is sufficient for their clinical applications. Indeed, neurological dysfunctions such as kernicterus or bilirubin encephalopathy may develop when the BR concentration rises above 0.03 mg/mL ($5 \times 10^{-5}$ M).[3] Jaundice can usually be detected when the serum bilirubin level exceeds 0.02 to 0.025 mg/mL (3.4 to 4.3 $\times 10^{-5}$ M). When the level of bilirubin is between 0.01 and 0.02 mg/mL (1.7 to 3.4 $\times 10^{-5}$ M), it is known as latent jaundice.[11] The various prominent analytical methods used for BR measurements are detailed in the work of Ngashangva et al.[45] According to the data presented, the SERS BR analysis method is not inferior in sensitivity to many previously proposed optical methods.

Figure 6a presents the point-to-point SERS reproducibility of the BR ($10^{-4}$ M) measurements within one map. The intensity of the characteristic peak of BR at 685 $cm^{-1}$ was examined for 100 spectra and plotted as a function of spectrum number. The relative standard deviation (RSD) is also shown on a picture as a light red area and is approximately 20%. The point-to-point SERS reproducibility of the BR with a concentration of $10^{-5}$ M is shown in Figure S5 and has a RSD of 27%. This demonstrates that the investigated SERS substrate is capable of generating SERS signals with good reproducibility.

Figure 6b demonstrates the signal variation for 5 different maps within the same substrate mentioned above. Each box represents 100 spectra of one map, and the outside points on the third and fifth scans most likely appear due to a slight depth difference during the map measurements. However, the variation demonstrates the good homogeneity of the substrate.

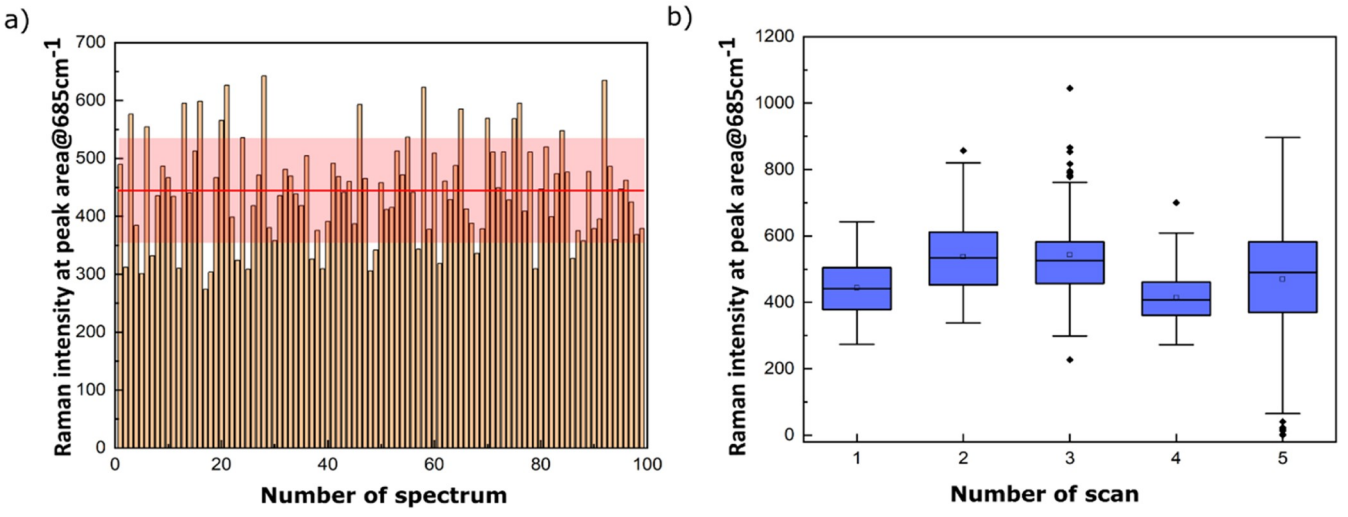


**Figure 6.** (a) Point-to-point SERS reproducibility of $10^{-4}$ M BR in PBS obtained from a 10 × 10 $\mu$m area with a 1 $\mu$m step. The red line shows the average intensity, and the light red area represents the standard deviation of the obtained spectra. (b) The scan-to-scan SERS reproducibility of 5 different scans consisting of 100 spectra. Blue boxes show standard deviation; error bars represent 95% confidence interval, and dots represent data outside the confidence interval.



https://doi.org/10.1021/acsbiomaterials.1c00728
ACS Biomater. Sci. Eng. 2022, 8, 4175−4184

Each box represents 100 spectra of one map. The ANOVA and post hoc Tukey honest significant difference (HSD) analyses are shown in the Supporting Information. The analysis shows that the results for different maps may be significantly different. This could be explained by nonhomogeneity of analyte deposition, variation of SiNW layer thickness, different focusing conditions, etc. However, the difference is not big; i.e., the mean intensity equals 480 arb. units, while the standard deviation is 50 arb. units. Thus, the reproducibility from map to map is estimated to be 10%.

Additionally, five batches of the substrates were prepared to investigate the batch-to-batch SERS reproducibility. Here, the substrate from each batch was investigated by measuring 100 spectra per substrate using a $10^{-4}$ M concentration of BR. Similarly, as for previous analyses, the peak area at 685 $cm^{-1}$ was calculated and plotted for individual batches of substrates (Figure S6). These investigations reveal that all batches of Au@SiNWs are SERS active and have a similar performance to the RSD for the mean of around 25%. This indicates the good reliability of the proposed method.

To measure the selectivity of the developed platform, the presence of BR was evaluated in a model solution with competing human serum albumin (HSA) molecules. According to the data presented in Figure S7, it can be seen that the SERS signal from HSA is practically absent, which indicates the absence of albumin binding to the Au@SiNW surface. At the same time, a clear presence of the SERS signal from BR was observed in the mixture of HSA and BR, which indicates the possibility of its determination in multicomponent solutions.

Artificial urine was used to gain insight into the effect of various parameters, such as matrix complexity, on the overall SERS BR signal. Figure 7 shows the mean SERS spectra of BR with a concentration of $5 \times 10^{-5}$ M, adsorbed on modified Au@SiNW substrates, and then stored in the dark at 4 °C; the mean SERS spectrum of the artificial urine; the Raman spectrum of the BR powder.

The SERS spectra in Figure 7 clearly show characteristic BR bands, which were retained during storage of the substrate for 7 days after its adsorption. The Raman signal of artificial urine shows a band at 990 $cm^{-1}$, which corresponds to the C−N stretching vibration of the urea.[34] Note that here the concentration of BR was $5 \times 10^{-5}$ M, which is the required sensitivity for clinical applications.

**Theoretical Analysis of SERS in SiNW and Au@SiNW Substrates.** To qualitatively study the optical properties of pure SiNW arrays and gold-decorated Au@SiNW arrays, we develop a three-dimensional model in COMSOL Multiphysics considering two types of structures (Figure 8). The first structure is a periodic array of SiNW with a 50 nm diameter of the nanowires, 400 nm height of the nanowires, and 120 nm height of the tapered part, and the distance between the nanowire axes is 80 nm, which is consistent with the SEM data in Figure 2. The second structure is the gold-decorated periodic array of Au@SiNW, where we cover the nanowires and c-Si substrate from the first model with 30 nm diameter gold spheres. We estimate the Raman enhancement factor in the described systems as

$$G_{\mathrm{Au@SiNW}} = \frac{1}{A}\iint_A \frac{|\mathbf{E}_{\mathbf{Au@SiNW}}|^4}{|\mathbf{E_0}|^4}\,dA,$$

$$G_{\mathrm{SiNW}} = \frac{1}{A}\iint_A \frac{|\mathbf{E}_{\mathbf{SiNW}}|^4}{|\mathbf{E_0}|^4}\,dA \qquad (1)$$

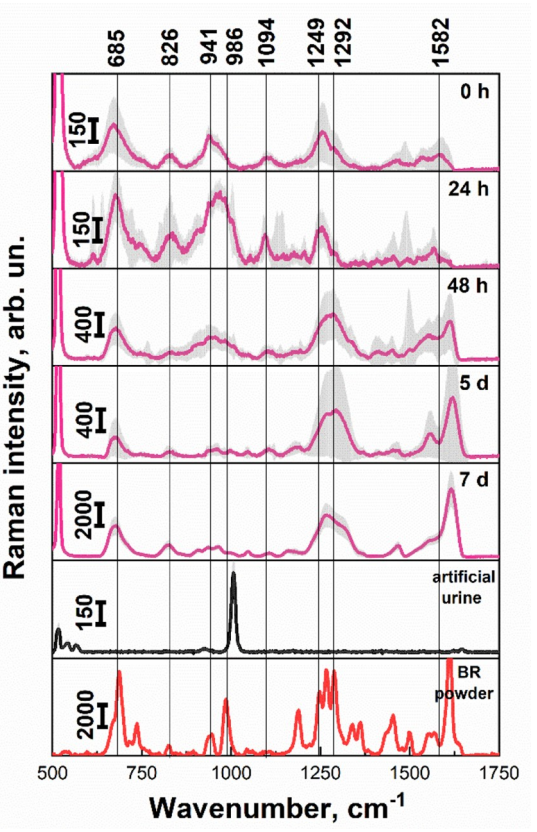


**Figure 7.** Average SERS spectra of BR with a concentration of $5 \times 10^{-5}$ M in artificial urine for Au@SiNWs at different storage times (0−7 days) after BR adsorption, average SERS spectrum of artificial urine, and Raman spectrum of BR powder. The gray shading in the average spectra shows the standard deviations calculated from about 100 spectra.

where $\mathbf{E}$ ($\mathbf{E_0}$) is a local (incident) electric field vector electromagnetic wave at the wavelength of the pump laser; the indices show the corresponding model, and $A$ is an integration surface with the shape of the nanowire repeated and placed 0.1 nm from the nanowire boundaries. Equation 1 implies that (a) the local intensity of Raman scattering is proportional to the local pump intensity; (b) the Raman shift is small compared to the pump wavelength and can be neglected in electromagnetic simulations.

The calculated electric field distribution for the first and second models is presented in Figure 8. The presence of plasmon resonances in the agglomerates of gold nanoparticles leads to a local enhancement of the field near their surfaces, the appearance of hot spots. As a result, the field scattered from the molecules attached to the silicon nanowire near the agglomerate is significantly enhanced. The values of the enhancement coefficient for the considered structures are estimated to be $G_{\mathrm{SiNW}} \sim 8.1$ and $G_{\mathrm{An@SiNW}} \sim 4 \times 10^8$, which means the presence of gold nanoparticles sufficiently increases the sensitivity of SERS. Therefore, the total enhancement obtained from the presence of gold is $\frac{G_{\mathrm{An@SiNW}}}{G_{\mathrm{SiNW}}} \sim 5 \times 10^7$.

## CONCLUSIONS

In summary, we have developed Au@SiNWs that could be used for the sensitive label-free SERS detection of free bilirubin. The SiNW arrays were created by gold-assisted



https://doi.org/10.1021/acsbiomaterials.1c00728
ACS Biomater. Sci. Eng. 2022, 8, 4175−4184

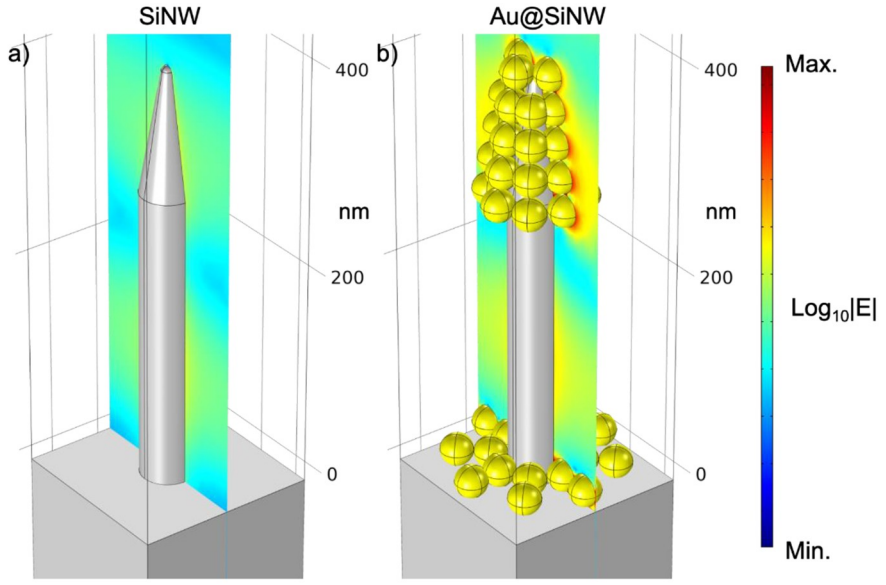


**Figure 8.** Calculated electric field distribution of the plane electromagnetic wave normally incident to (a) a periodic SiNW substrate; (b) a periodic An@SiNW substrate. Color shows the value of $\log_{10}(|\mathbf{E}|)$, where **E** is an electric field vector. Calculations are made for $\lambda$ = 633 nm.

chemical etching and then were additionally decorated with Au NPs using their simple reduction on crystalline silicon from $AuCl_3$ in the presence of HF. To the best of our knowledge, this is the first time such a method for making the gold-decorated SiNW substrates has been proposed. This fabrication method has a short processing time, is cost-effective, and provides structural variability with a high potential for SERS applications. The obtained substrates demonstrated a great SERS response for the model molecule, 4-MPy, which was successfully detected down to a concentration of $10^{-8}$ M with an excellent homogeneous signal. For effective absorption of the hydrophobic, negatively charged BR molecule, a simple method has been proposed to modify the surface of SiNWs with amino groups. This provided a positive charge on the surface of the nanowires. We developed a theoretical model in COMSOL Multiphysics to study the influence of the gold decoration of SiNW substrates on SERS effectiveness. We showed that the excitation of plasmons in Au NPs increases the local field, which leads to a strong enhancement of the local Raman response. The value of the total Raman enhancement factor for the structure in the study exceeds $5 \times 10^7$, which indicates a significant enhancement of SERS sensitivity in the presence of a gold coat. Since gold nanoparticles are located both at the top and at the bottom of the nanowires, this makes it possible to record the signal of analyte molecules adsorbed on the SiNWs. Thus, the presented theoretical calculations confirm the success of the SERS detection of BR adsorbed directly on the modified surface of the nanowires. According to the data presented, BR was successfully detected down to the concentration of $10^{-6}$ M with high point-to-point, scan-to-scan, and batch-to batch reproducibility by using the modified Au@SiNW substrates. Note that such signal detection sensitivity is required for clinical applications. The obtained results open the possibility of using SERS-active Au@SiNW substrates as platforms for point-of-care label-free clinical diagnostics of bilirubin.

## ■ ASSOCIATED CONTENT

### Supporting Information

The Supporting Information is available free of charge at https://pubs.acs.org/doi/10.1021/acsbiomaterials.1c00728.

Energy dispersive X-ray fluorescence spectra of SiNW and Au@SiNW substrates; ANOVA (analysis of variance) and post hoc Tukey HSD analysis data; average SERS spectra of 4-MPy with a concentration of $10^{-8}$ M adsorbed on the Au@SiNW substrate, and of 4-MPy, $10^{-5}$ M, adsorbed on the SiNW substrate; LOD estimation; Raman spectra; batch-to-batch SERS reproducibility of 5 different batches consisting of 100 spectra; point-to-point SERS reproducibility of $10^{-5}$ M BR in PBS obtained from 10 × 10 $\mu$m area with a 1 $\mu$m step; average SERS spectra of HSA ($10^{-4}$ M) and BR ($10^{-5}$ M) solutions (PDF)

## ■ AUTHOR INFORMATION


### Corresponding Author

**Liubov A. Osminkina** − *Lomonosov Moscow State University, Faculty of Physics, 119991 Moscow, Russia; Institute for Biological Instrumentation of Russian Academy of Sciences, 142290 Pushchino, Moscow Region, Russia;* orcid.org/0000-0001-7485-0495; Email: osminkina@physics.msu.ru

### Authors

**Anna D. Kartashova** − *Lomonosov Moscow State University, Faculty of Physics, 119991 Moscow, Russia*

**Kirill A. Gonchar** − *Lomonosov Moscow State University, Faculty of Physics, 119991 Moscow, Russia*

**Dmitry A. Chermoshentsev** − *Skolkovo Institute of Science and Technology, Center for Photonics and Quantum Materials, 143025 Moscow, Russia; Moscow Institute of Physics and Technology, 141701 Moscow, Russia; Russian Quantum Center, 143025 Moscow, Russian Federation*

**Ekaterina A. Alekseeva** − *Lomonosov Moscow State University, Faculty of Physics, 119991 Moscow, Russia*




https://doi.org/10.1021/acsbiomaterials.1c00728
ACS Biomater. Sci. Eng. 2022, 8, 4175−4184

**Maxim B. Gongalsky** − *Lomonosov Moscow State University, Faculty of Physics, 119991 Moscow, Russia;* orcid.org/0000-0002-7069-4234

**Ivan V. Bozhev** − *Lomonosov Moscow State University, Faculty of Physics, 119991 Moscow, Russia; Quantum Technology Center, Lomonosov Moscow State University, 119991 Moscow, Russia*

**Andrei A. Eliseev** − *Lomonosov Moscow State University, Faculty of Chemistry, 119991 Moscow, Russia;* orcid.org/0000-0002-2851-6821

**Sergey A. Dyakov** − *Skolkovo Institute of Science and Technology, Center for Photonics and Quantum Materials, 143025 Moscow, Russia;* orcid.org/0000-0002-3729-6621

**Jeanne V. Samsonova** − *Lomonosov Moscow State University, Faculty of Physics, 119991 Moscow, Russia; Lomonosov Moscow State University, Faculty of Chemistry, 119991 Moscow, Russia*

Complete contact information is available at: https://pubs.acs.org/10.1021/acsbiomaterials.1c00728

### Notes

The authors declare no competing financial interest.

## ■ ACKNOWLEDGMENTS

The research was funded by the Russian Science Foundation (grant number 20-12-00297). This research was performed according to the Development Program of the Interdisciplinary Scientific and Educational School of Lomonosov Moscow State University "Photonic and quantum technologies: Digital medicine". The equipment of the "Educational and Methodical Center of Lithography and Microscopy", M.V. Lomonosov Moscow State University Research Facilities Sharing Centre, was used.

## ■ ABBREVIATIONS

BR, bilirubin; SERS, surface-enhanced Raman scattering; Au@SiNWs, gold-decorated silicon nanowires; SiNWs, silicon nanowires; Au NPs, gold nanoparticles; 4-MPy, 4-mercaptopyridine; MACE, metal-assisted chemical etching; HF, hydrofluoric acid; $H_2O_2$, hydrogen peroxide; $AuCl_3$, gold(III) chloride; RT, room temperature; APRES, 3-aminopropyl-(triethoxyl)silane; PBS, phosphate-buffered saline; WCA, water contact angle

## ■ REFERENCES

(1) Avramescu, M. E.; Sager, W. F. C.; Borneman, Z.; Wessling, M. Adsorptive membranes for bilirubin removal. *J. Chromatogr. B: Anal. Technol. Biomed. Life Sci.* **2004**, *803* (2), 215−223.

(2) Brodersen, R.; Stern, L. Binding of bilirubin to albumin. *Crc critical reviews in clinical laboratory sciences* **1980**, *11* (4), 307−399.

(3) American Academy of Pediatrics. Practice parameter: management of hyperbilirubinemia in the healthy term newborn. *Pediatrics* **1994**, *94*, 558−565.

(4) Watchko, J. F. Kernicterus and the molecular mechanisms of bilirubin-induced CNS injury in newborns. *NeuroMol. Med.* **2006**, *8* (4), 513−529.

(5) Kaplan, M.; Hammerman, C. Understanding severe hyperbilirubinemia and preventing kernicterus: adjuncts in the interpretation of neonatal serum bilirubin. *Clin. Chim. Acta* **2005**, *356* (1−2), 9−21.

(6) Roche, S. P.; Kobos, R. Jaundice in the adult patient. *Am. Fam. Physician* **2004**, *69* (2), 299−304.

(7) Pan, X.; Li, L.; Lin, H.; Tan, J.; Wang, H.; Liao, M.; Chen, C.; Shan, B.; Chen, Y.; Li, M. A graphene oxide-gold nanostar hybrid based-paper biosensor for label-free SERS detection of serum bilirubin for diagnosis of jaundice. *Biosens. Bioelectron.* **2019**, *145*, 111713.

(8) Hooda, V.; Gahlaut, A.; Gothwal, A.; Hooda, V. Bilirubin enzyme biosensor: potentiality and recent advances towards clinical bioanalysis. *Biotechnol. Lett.* **2017**, *39* (10), 1453−1462.

(9) Mayer, M. Association of serum bilirubin concentration with risk of coronary artery disease. *Clin. Chem.* **2000**, *46* (11), 1723−1727.

(10) Khan, M. M.; Tayyab, S. Understanding the role of internal lysine residues of serum albumins in conformational stability and bilirubin binding. *Biochim. Biophys. Acta, Protein Struct. Mol. Enzymol.* **2001**, *1545* (1−2), 263−277.

(11) Puppalwar, P. V.; Goswami, K.; Dhok, A. Review on "evolution of methods of bilirubin estimation. *IOSR Journal of Dental and Medical Sciences* **2012**, *1* (3), 17−28.

(12) Hajzer, Š. Comparison of direct spectrophotometric determinations of bilirubin with candidate reference method in sera of newborns. *Clin. Chem. Lab. Med.* **1989**, *27* (7), 445−449.

(13) Winsten, S.; Cehelyk, B. A rapid micro diazo technique for measuring total bilirubin. *Clin. Chim. Acta* **1969**, *25* (3), 441−446.

(14) Kazmierczak, S. C.; Robertson, A. F.; Catrou, P. G.; Briley, K. P.; Kreamer, B. L.; Gourley, G. R. Direct spectrophotometric method for measurement of bilirubin in newborns: comparison with HPLC and an automated diazo method. *Clin. Chem.* **2002**, *48* (7), 1096−1097.

(15) Langer, J.; et al. Present and future of surface-enhanced Raman scattering. *ACS Nano* **2020**, *14*, 28−117.

(16) Zheng, X. S.; Jahn, I. J.; Weber, K.; Cialla-May, D.; Popp, J. Label-free SERS in biological and biomedical applications: recent progress, current challenges and opportunities. *Spectrochim. Acta, Part A* **2018**, *197*, 56−77.

(17) Saviñon-Flores, F.; Méndez, E.; López-Castaños, M.; Carabarin-Lima, A.; López-Castaños, K. A.; González-Fuentes, M. A.; Méndez-Albores, A. A Review on SERS-Based Detection of Human Virus Infections: Influenza and Coronavirus. *Biosensors* **2021**, *11* (3), 66.

(18) Fleischmann, M.; Hendra, P. J.; McQuillan, A. J. Raman spectra of pyridine adsorbed at a silver electrode. *Chem. Phys. Lett.* **1974**, *26* (2), 163−166.

(19) Moskovits, M. Surface-enhanced spectroscopy. *Rev. Mod. Phys.* **1985**, *57* (3), 783.

(20) Zou, Y.; Zhang, Y.; Xu, Y.; Chen, Y.; Huang, S.; Lyu, Y.; Duan, H.; Chen, Z.; Tan, W. Portable and label-free detection of blood bilirubin with graphene-isolated-Au-nanocrystals paper strip. *Anal. Chem.* **2018**, *90* (22), 13687−13694.

(21) Geng, Z. Q.; Xu, D.; Song, Y.; Wang, W. P.; Li, Y. P.; Han, C. Q.; Yang, G. H.; Qu, L. L.; Ajayan, P. M. Sensitive label-free detection of bilirubin in blood using boron nitride-modified nanorod arrays as SERS substrates. *Sens. Actuators, B* **2021**, *334*, 129634.

(22) Pan, X.; Li, L.; Lin, H.; Tan, J.; Wang, H.; Liao, M.; Chen, C.; Shan, B.; Chen, Y.; Li, M. A graphene oxide-gold nanostar hybrid based-paper biosensor for label-free SERS detection of serum bilirubin for diagnosis of jaundice. *Biosens. Bioelectron.* **2019**, *145*, 111713.

(23) Xu, D.; Duan, L.; Jia, W.; Yang, G.; Gu, Y. Fabrication of Ag@Fe2O3 hybrid materials as ultrasensitive SERS substrates for the detection of organic dyes and bilirubin in human blood. *Microchem. J.* **2021**, *161*, 105799.

(24) Chiappini, C.; Liu, X.; Fakhoury, J. R.; Ferrari, M. Biodegradable porous silicon barcode nanowires with defined geometry. *Adv. Funct. Mater.* **2010**, *20* (14), 2231−2239.

(25) Georgobiani, V. A.; Gonchar, K. A.; Zvereva, E. A.; Osminkina, L. A. Porous silicon nanowire arrays for reversible optical gas sensing. *Phys. Status Solidi A* **2018**, *215* (1), 1700565.

(26) Arshavsky-Graham, S.; Massad-Ivanir, N.; Segal, E.; Weiss, S. Porous silicon-based photonic biosensors: Current status and emerging applications. *Anal. Chem.* **2019**, *91* (1), 441−467.

(27) Zukovskaja, O.; Agafilushkina, S.; Sivakov, V.; Weber, K.; Cialla-May, D.; Osminkina, L.; Popp, J. Rapid detection of the

bacterial biomarker pyocyanin in artificial sputum using a SERS-active silicon nanowire matrix covered by bimetallic noble metal nanoparticles. *Talanta* **2019**, *202*, 171−177.
(28) Alhmoud, H.; Brodoceanu, D.; Elnathan, R.; Kraus, T.; Voelcker, N. H. A MACEing silicon: Towards single-step etching of defined porous nanostructures for biomedicine. *Prog. Mater. Sci.* **2021**, *116*, 100636.
(29) Mariani, S.; Paghi, A.; La Mattina, A. A.; Debrassi, A.; Dahne, L.; Barillaro, G. Decoration of porous silicon with gold nanoparticles via layer-by-layer nanoassembly for interferometric and hybrid photonic/plasmonic (bio) sensing. *ACS Appl. Mater. Interfaces* **2019**, *11* (46), 43731−43740.
(30) Mariani, S.; Robbiano, V.; Strambini, L. M.; Debrassi, A.; Egri, G.; Dähne, L.; Barillaro, G. Layer-by-layer biofunctionalization of nanostructured porous silicon for high-sensitivity and high-selectivity label-free affinity biosensing. *Nat. Commun.* **2018**, *9* (1), 5256.
(31) Huang, Z.; Geyer, N.; Werner, P.; De Boor, J.; Gösele, U. Metal-assisted chemical etching of silicon: a review: in memory of Prof. Ulrich Gösele. *Adv. Mater.* **2011**, *23* (2), 285−308.
(32) Loza, K.; Diendorf, J.; Sengstock, C.; Ruiz-Gonzalez, L.; Gonzalez-Calbet, J. M.; Vallet-Regi, M.; Köller, M.; Epple, M. The dissolution and biological effects of silver nanoparticles in biological media. *J. Mater. Chem. B* **2014**, *2* (12), 1634−1643.
(33) Majoul, N.; Aouida, S.; Bessaïs, B. Progress of porous silicon APTES-functionalization by FTIR investigations. *Appl. Surf. Sci.* **2015**, *331*, 388−391.
(34) Hidi, I. J.; Jahn, M.; Pletz, M. W.; Weber, K.; Cialla-May, D.; Popp, J. Toward levofloxacin monitoring in human urine samples by employing the LoC-SERS technique. *J. Phys. Chem. C* **2016**, *120* (37), 20613−20623.
(35) Osminkina, L. A.; Zukovskaja, O.; Agafilushkina, S. N.; Kaniukov, E.; Stranik, O.; Gonchar, K. A.; Yakimchuk, D.; Bundyukova, V.; Chermoshentsev, D. A.; Dyakov, S. A.; Gippius, N. A.; Weber, K.; Popp, J.; Cialla-May, D.; Sivakov, V. Gold nanoflowers grown in a porous Si/SiO2 matrix: The fabrication process and plasmonic properties. *Appl. Surf. Sci.* **2020**, *507*, 144989.
(36) Guo, H.; Ding, L.; Mo, Y. J. Adsorption of 4-mercaptopyridine onto laser-ablated gold, silver and copper oxide films: A comparative surface-enhanced Raman scattering investigation. *J. Mol. Struct.* **2011**, *991*, 103−107.
(37) Agafilushkina, S. N.; Žukovskaja, O.; Dyakov, S. A.; Weber, K.; Sivakov, V.; Popp, J.; Cialla-May, D.; Osminkina, L. A. Raman Signal Enhancement Tunable by Gold-Covered Porous Silicon Films with Different Morphology. *Sensors* **2020**, *20* (19), 5634.
(38) Zucker, S. D.; Goessling, W.; Hoppin, A. G. Unconjugated bilirubin exhibits spontaneous diffusion through model lipid bilayers and native hepatocyte membranes. *J. Biol. Chem.* **1999**, *274* (16), 10852−10862.
(39) Wu, G.; Brown, G. R. Adsorption of bilirubin by amine-containing polyacrylamide resins. *React. Polym.* **1991**, *14* (1), 49−61.
(40) Majoul, N.; Aouida, S.; Bessaïs, B. Progress of porous silicon APTES-functionalization by FTIR investigations. *Appl. Surf. Sci.* **2015**, *331*, 388−391.
(41) Culler, S. R.; Ishida, H.; Koenig, J. L. Structure of silane coupling agents adsorbed on silicon powder. *J. Colloid Interface Sci.* **1985**, *106* (2), 334−346.
(42) Celis, F.; Campos-Vallette, M. M.; Gómez-Jeria, J. S.; Clavijo, R. E.; Jara, G. P.; Garrido, C. Surface-enhanced Raman scattering and theoretical study of the bilichromes biliverdin and bilirubin. *Spectrosc. Lett.* **2016**, *49* (5), 336−342.
(43) Rai, A. K.; Rai, S. B.; Rai, D. K.; Singh, V. B. Spectroscopic studies and normal coordinate analysis of bilirubin. Spectrochimica Acta Part A: *Spectrochim. Acta, Part A* **2002**, *58* (10), 2145−2152.
(44) Yang, B.; Taylor, R. C.; Morris, M. D.; Wang, X. Z.; Wu, J. G.; Yu, B. Z.; Xu, G.; Soloway, R. D. Normal coordinate analysis of bilirubin vibrational spectra: effects of intramolecular hydrogen bonding. *Spectrochimica Acta Part A: Molecular Spectroscopy* **1993**, *49* (12), 1735−1749.
(45) Ngashangva, L.; Bachu, V.; Goswami, P. Development of new methods for determination of bilirubin. *J. Pharm. Biomed. Anal.* **2019**, *162*, 272−285.




https://doi.org/10.1021/acsbiomaterials.1c00728
*ACS Biomater. Sci. Eng.* 2022, 8, 4175−4184